Immunopeptidome mining reveals a novel ERS-induced target in T1D

Lina Wang
Army Medical University(Third Military Medical University)
Jie Li
Army Medical University(Third Military Medical University)
Shushu Yang
Army Medical University(Third Military Medical University)
Gang Meng
Southwest Hospital, Army Medical University (Third Military Medical University)
Xiaoling Chen
Army Medical University (Third Military Medical University)
Zhang Mengjun
Army Medical University
Wang Shufeng
Army Medical University
Xiangqian Li
Army Medical University (Third Military Medical University)
Yuzhang Wu
Third Military Medical University
Li Wang
liwang118@tmmu.edu.cn

Army Medical University(Third Military Medical University)

Article

Keywords:

Posted Date: June 9th, 2023

DOI: https://doi.org/10.21203/rs.3.rs-2997556/v1

Additional Declarations: (Not answered)

Version of Record: A version of this preprint was published at Cellular & Molecular Immunology on April 30th, 2024. See the published version at https://doi.org/10.1038/s41423-024-01150-0.

Abstract

Autoreactive $CD8^+$ T cells play a key role in type 1 diabetes (T1D), but the antigen spectrum that activates autoreactive $CD8^+$ T cells remains unclear. Endoplasmic reticulum stress (ERS) has been implicated in β cell autoantigen generation. Here, we analyzed the major histocompatibility complex class I (MHC-I)-associated immunopeptidome (MIP) of islet β cells under steady-state and ERS conditions and found a small number of peptides that were exclusively present in the MIP of the ERS-exposed β cell line. Among them, $OTUB2_{58-66}$ showed immunodominance, and the corresponding autoreactive $CD8^+$ T cells were diabetogenic in NOD mice. High glucose intake upregulated pancreatic OTUB2 expression and amplified the $OTUB2_{58-66}$-specific $CD8^+$ T-cell response in NOD mice. Repeated $OTUB2_{58-66}$ administration significantly reduced the T1D incidence in these mice. This study provides novel β cell autoantigens for developing specific immune interventions for T1D prevention and treatment. Data are available via ProteomeXchange with identifier PXD041227.

INTRODUCTION

Type 1 diabetes (T1D) is an organ-specific autoimmune disease mainly caused by the destruction of islet β cells by self-reactive T cells. Globally, the incidence of T1D has increased by an average annual rate of 3 ~ 4% over the past three decades, and while this disease can occur at any age, the incidence peaks in the age range of approximately 10 ~ 14 years old (1). Although supplemental insulin therapy is well established, there is no radical treatment for T1D, and patients with T1D remain at high risk of serious complications, so T1D is still a great threat to adolescents (2). Autoreactive $CD8^+$ T cells play a key role in the pathogenesis of T1D (3). $CD8^+$ T cells are the first effector cells to infiltrate the islets and destroy β cells (4). Autoreactive $CD8^+$ T cells attack islet β cells by specifically recognizing self-peptides presented by major histocompatibility complex class I (MHC-I) molecules on the cell surface (5). MHC class I genes were identified as T1D susceptibility genes independent of MHC class II alleles (6). Nonobese diabetic (NOD) mice with MHC-I, β2-microglobulin or CD8α gene deletion do not develop T1D, and adoptive transfer of pancreas-infiltrating $CD8^+$ T cells from NOD mice into nonobese diabetes/severe combined immunodeficiency (NOD/scid) mice can induce T1D onset(7).

To date, the β cell autoantigen spectrum that drives autoreactive $CD8^+$ T-cell responses in T1D is not completely elucidated. The collection of peptides presented by MHC-I molecules is called the MHC-I-associated immunopeptidome (MIP), and its composition is variable but precisely regulated by intrinsic and extrinsic cellular factors (8). The emerging self-peptides in the MIP induced by certain pathological factors may contain targets for $CD8^+$ T-cell recognition and response (9). However, thus far, direct identification of self-peptide ligands derived from the β cell MIP and recognized by autoreactive $CD8^+$ T cells has been limited in T1D studies.

Endoplasmic reticulum stress (ERS) is a self-protective cellular mechanism that activates the unfolded protein response (UPR) in response to misfolded or unfolded protein aggregation in the ER lumen (10).

However, pathological ERS that is overly strong or prolonged can cause cell dysfunction and apoptosis, which are closely related to the occurrence and development of many diseases, including T1D (11, 12). Islet β cells are endocrine cells with an abundant ER system that folds, transports and processes newly synthesized insulin in response to changes in the blood glucose level in real time, which makes islet β cells extremely sensitive to ERS (13). Many environmental factors, including viral infection (14), chemical factors (15), reactive oxygen species (16), hyperglycemia (17), and inflammation (18), can evoke pathological ERS in β cells. For example, high sugar consumption has been suggested as a potential environmental risk factor closely related to T1D progression (19). Our recent study demonstrated that high glucose intake accelerated T1D onset in NOD mice by causing abnormal ERS in islet β cells and enhancing the visibility of islet β cells to the immune system (20).

There is growing evidence showing an association between pathological ERS and increased visibility of β cells to the immune system. Recent studies have demonstrated that pathological ERS can produce “neo-autoantigens” in islet β cells via abnormal modification (21), gene mRNA open reading frame shift (22) and discontinuous peptide fragment splicing (23). However, the conventional self-peptides that are naturally processed and presented by MHC-I molecules in β cells in a pathological ERS state, especially those recognized by autoreactive $CD8^+$ T cells, have been largely ignored. Here, by comparative analysis of the landscape of the MIP derived from a NOD mouse β cell line under steady-state and ERS-state conditions, we discovered a novel ERS-associated conventional diabetogenic self-peptide derived from the ubiquitin thioesterase OTUB2 based on its exclusive representation in the β cell line MIP derived under ERS.

RESULTS

High-glucose or thapsigargin treatment reshapes the MIP of NIT-1 β cells and generates novel conventional peptides naturally presented by MHC class I molecules

To investigate whether ERS induction could enhance the visibility of β cells to peripheral $CD8^+$ T cells from NOD mice, a NOD mouse-derived β cell line, NIT-1, was pretreated with high glucose (HG) or the classic ERS inducer thapsigargin (TG) and then cocultured with NOD mouse splenocytes lacking $CD4^+$ T cells for 24 h. IFN-γ ELISPOT analysis showed that NIT-1 cells pretreated with 20 mM HG for 24 h had the strongest ability to stimulate NOD mouse $CD4^-$ splenocytes to secrete IFN-γ (Fig. S1A, 1B), while treatment with 5 μM TG for 0.5 h also significantly enhanced the immune visibility of NIT-1 cells (Fig. S1D,1E). These responses were significantly weakened by an anti-H-2Kd antibody (Fig.S1C, 1F), indicating that NIT-1-stimulated IFN-γ secretion by NOD mouse $CD4^-$ splenocytes was primarily MHC class I molecule dependent. However, HG or TG treatment did not induce significant changes in the level of MHC class I molecules on the surface of NIT-1 cells (Fig. S1G). Furthermore, quantitative real-time PCR (qPCR) and western blot results confirmed that both HG treatment and TG treatment effectively induced sustained and enhanced ERS in NIT-1 cells (Fig. S1H, 1I). Tauroursodeoxycholic acid (TUDCA), a

classic ERS inhibitor, significantly weakened the HG- and TG-induced increases in the immune visibility of NIT-1 cells to NOD mouse splenocytes (Fig. S1J).

Given that $CD8^+$ T cells respond to target cells by scanning the MIP of target cells through T cell receptors, we then questioned whether the increased visibility of ER-stressed NIT-1 β cells to $CD8^+$ T cells from NOD mice was due to changes in their MIP induced by HG or TG treatment. To establish a dataset for the β cell-derived MIP, nonstressed NIT-1 cells (NIT-1-NC) or NIT-1 cells with ERS induced by HG (NIT-1-HG) or TG (NIT-1-TG) were lysed for immunopurification of peptide-MHC-I complexes. The MHC-I-bound peptides were then acid-eluted and analyzed by liquid chromatography-tandem mass spectrometry (LC—MS/MS) (Fig. 1A). By matching the MS spectra against a custom mouse MHC-I targeted peptide database we previously established with no cleavage at a false discovery rate (FDR) of 5% (24), we ultimately obtained a total of 214, 219 and 314 unique conventional H-2Kd–restricted peptides probably from 198, 203 and 292 source proteins in the MIP of the NIT-1-NC, NIT-1-HG and NIT-1-TG groups, respectively (Fig. 1B and Supplementary Table 1). The identified peptides were mainly 9 amino acids in length (Fig. 1C); most (> 80%) were predicted to be strong H-2Kd binders (SB) with a rank < 0.5% (NetMHC) (Fig. 1D) and showed a typical H-2Kd-binding motif with tyrosine and leucine or isoleucine as the main anchor residues on P2 and P9, respectively (Fig. 1E). These data indicated that the NIT-1 cell-derived H-2Kd-restricted MIP datasets were highly reliable. Unfortunately, we identified only a much smaller number of H-2Db-restricted peptides in the NIT-1 cell-derived MIP (Fig. S2A), possibly because the expression level of Db was much lower than that of Kd in NIT-1 cells (Fig. S1G). This was consistent with the Kd and Db expression patterns in NOD mouse pancreas tissues; in contrast, there is almost no biased expression of H-2Kd and Db molecules on the surface of BALB/c mouse thymus cells (24). The majority of the H-2Db-restricted peptides were 9 amino acids in length (Fig. S2B), but most of them (> 60%) were predicted to be weak binders (WB) (Fig. S2C). The SB peptides also showed a typical H-2Db-binding motif with asparagine and phenylalanine or glutamic acid as the main anchor residues on P5 and P9, respectively (Fig. S2D). Therefore, we mainly focused on the H-2Kd-restricted peptides in subsequent studies.

By overlapping the H-2Kd-restricted MIP landscapes of NIT-1-NC, NIT-1-HG and NIT-1-TG cells at the source protein level, we found that HG and TG treatments changed the composition of the NIT-1 cell-derived MIP to varying degrees (Fig. 1F). Notably, at the source protein level, a panel of H-2Kd-restricted self-peptides was exclusively present in the MIP of ER-stressed NIT-1 β cells treated with either HG or TG but not in that of nonstressed NIT-1 β cells (Fig. 1G and Supplementary Table 2). Together, these results suggest that ERS induction significantly increases the visibility of NIT-1 β cells to peripheral $CD8^+$ T cells from NOD mice and simultaneously generates a novel panel of conventional self-peptides naturally presented by MHC class I molecules on NIT-1 β cells.

$OTUB2_{58-66}$ is an immunodominant self-peptide in NOD mice

We then questioned whether the enhanced immune visibility of ER-stressed NIT-1 cells to $CD8^+$ T cells was related to the MHC-I peptides that exclusively emerged in ERS-state NIT-1 cells. To test the immunogenicity of these self-peptides, a recall IFN-γ ELISPOT assay was performed (Fig. 2A). The dendritic cells (DCs) used in this analysis were generated from NOD mouse bone marrow and showed good purity and maturity (Fig. S3). Compared with DCs alone, DCs pulsed with the peptide $WDR70_{530-538}$, $SYT12_{291-299}$ or $OTUB2_{58-66}$ stimulated more IFN-γ production in NOD mouse $CD4^-$ splenocytes primed with the corresponding peptide, and these responses were effectively weakened by anti-H-2Kd antibody treatment (Fig. 2B, 2C), indicating that peptide-induced IFN-γ production was primarily mediated by H-2Kd-restricted $CD8^+$ T cells. The MS identification accuracy for these three peptides was basically confirmed by comparing the secondary tandem MS data for the identified endogenous peptides with those for the synthetic peptides (Fig. S4). Furthermore, we evaluated the reactivity of splenocytes from NOD mice at different ages against these three self-peptides and $IGRP_{206-214}$, a reported H-2Kd-restricted immunodominant epitope. We found that 87.5% of the NOD mice responded positively to the peptide $OTUB2_{58-66}$ and almost half of the NOD mice responded positively to $WDR70_{530-538}$ and $SYT12_{291-299}$, but only 25% of the NOD mice showed a positive response to $IGRP_{206-214}$ (Fig. 2D). Collectively, these results suggest that the $OTUB2_{58-66}$ peptide represents a potential immunodominant self-peptide ligand of autoreactive $CD8^+$ T cells in NOD mice.

$OTUB2_{58-66}$-specific $CD8^+$ T cells are present and diabetogenic in NOD mice

To validate the presence of $OTUB2_{58-66}$-specific $CD8^+$ T cells in NOD mice, H-2Kd-peptide dextramer staining was performed, and the gating strategy is shown in Fig. S5A. The frequency of $CD8^+$ T cells recognizing $OTUB2_{58-66}$ was similar to or even higher than that of $CD8^+$ T cells recognizing $IGRP_{206-214}$ peptides in the spleen, pancreas and pancreatic draining lymph nodes (pLNs) of NOD mice (Fig. 3A). However, the frequencies of $IGRP_{206-214}$ and $OTUB2_{58-66}$ $Dextramer^+$ $CD8^+$ T cells were extremely low in the spleen of ICR mice, a nondiabetic control for NOD mice (Fig. S5B). The cytotoxicity marker CD107 was weakly expressed on splenic $CD8^+Dextramer^+$ T cells of ICR mice (Fig. S5C) but highly expressed on those of NOD mice (Fig.S5D). In NOD mice, the majority of splenic $CD8^+Dextramer^+$ T cells showed the $CD62L^+$ $CD44^+$ phenotype of central memory T cells, with the next biggest population being $CD62L^+$ $CD44^-$ naïve-like cells, while pancreas-infiltrating $CD8^+Dextramer^+$ T cells mainly showed the $CD62L^-$ $CD44^+$ phenotype of effector or effector memory T cells. Furthermore, the phenotype of $CD8^+Dextramer^+$ T cells in the pancreatic draining lymph nodes (pLN) was in between these results (Fig. S5E), indicating that the majority of $CD8^+Dextramer^+$ T cells were antigen-experienced in NOD mice. As expected, the $OTUB2_{58-66}$ peptide was capable of triggering the proliferation of endogenous splenic $CD8^+$ T cells in NOD mice (Fig. 3B, 3C). Compared with unloaded splenocytes (target control), $OTUB2_{58-66}$-loaded splenocytes (target cells) were more efficiently killed by splenic $CD8^+$ T cells (effector cells) freshly purified from NOD mice (Fig. 3D, 3E).

We then wanted to explore whether $OTUB2_{58-66}$-specific $CD8^+$ T cells are diabetogenic in vivo. NOD mice were subcutaneously immunized with $OTUB2_{58-66}$ mixed with the adjuvant polyinosine cytidine acid (poly IC), a Toll-like receptor 3 (TLR-3) agonist ($OTUB2_{58-66}$ group) or with poly IC alone (control group). Then, 7 days later, splenocytes were isolated from the immunized NOD mice, restimulated with the $OTUB2_{58-66}$ peptide or PBS, and then adoptively transferred into NOD/scid recipient mice (Fig. 4A). Analysis of the insulitis score and incidence of diabetes showed that the NOD/scid mice transferred with $OTUB2_{58-66}$-activated splenocytes developed severe insulitis and diabetes, while the NOD/scid mice receiving control splenocytes exhibited no obvious insulitis and were diabetes-free (Fig. 4B-D). Confocal microscopy results of immunofluorescence staining for CD8 and insulin revealed obvious infiltration of $CD8^+$ T cells in the local islets in the NOD/scid mice receiving $OTUB2_{58-66}$-activated splenocytes, while the control recipients had almost no $CD8^+$ T-cell infiltration in the islets (Fig. 4E). Collectively, these results show that endogenous $CD8^+$ T cells in NOD mice can recognize and respond to the H2-Kd-naturally presented $OTUB2_{58-66}$ self-peptide of islet β cells, ultimately exerting a diabetogenic effect.

High glucose intake amplifies $OTUB2_{58-66}$-specific $CD8^+$ T-cell responses in NOD mice.

Given our previous findings that high glucose intake accelerates T1D in NOD mice (25), and the results showing that the peptide $OTUB2_{58-66}$ could be a novel ERS-associated islet β cell self-peptide induced by high glucose, we wondered whether high glucose intake amplified the $OTUB2_{58-66}$-specific $CD8^+$ T-cell response in NOD mice. To this end, NOD mice were fed high-glucose water (20% glucose, HG) or normal water (NC) from 4 weeks of age and sacrificed at 6 or 12 weeks of age. Then, pancreas-infiltrating lymphocytes and splenocytes were isolated from the NOD mice for dextramer and intracellular cytokine staining. The results showed that the absolute number of pancreas-infiltrating lymphocytes in NOD mice in the HG group was significantly higher than that in NOD mice in the NC group at both 6 and 12 weeks of age (Fig. 5A) and that the frequency of $CD8^+$ $OTUB2_{58-66}$-$dextramer^+$ T cells in the pancreas of NOD mice in the HG group showed an increasing trend (Fig. 5B,5C). Intracellular cytokine staining showed that the secretion of IFN-γ and TNF-α by splenocytes from NOD mice in the HG group was significantly higher than that by splenocytes from NOD mice in the NC group at both 6 and 12 weeks of age upon either PMA or $OTUB2_{58-66}$ stimulation (Fig. 5D-F). Together, these results indicate that high glucose intake amplifies the response of $OTUB2_{58-66}$-autoreactive T cells in NOD mice. Then, we questioned whether the amplified $OTUB2_{58-66}$-specific $CD8^+$ T-cell responses in NOD mice given high-glucose water were due to increased expression of OTUB2 in β cells. Interestingly, we found that OTUB2 expression was increased in the pancreatic islets of NOD mice (Fig. 5G). As expected, the protein level of OTUB2 in the pancreas of NOD mice in the HG group was significantly higher than that in the NC group (Fig. 5H, 5I). Consistently, both HG and TG treatments increased the protein expression of OTUB2, although to different degrees, in NIT-1 β cells (Fig. 5J, 5K). However, the upregulation of OTUB2 induced by HG or TG was almost completely eliminated by TUDCA (Fig. 5L). Therefore, we speculate that high glucose intake may aggravate pathological ERS, upregulate OTUB2 expression and promote MHC-I

presentation of OTUB2$_{58-66}$ peptides in islet β cells, thereby amplifying OTUB2$_{58-66}$-autoreactive CD8$^+$ T-cell responses and ultimately promoting the progression of T1D.

Repeated administration of the OTUB2$_{58-66}$ peptide prevents T1D onset in NOD mice

Given that induction of autoreactive T-cell tolerance by administration of autoantigens or peptides may prevent autoimmune disease, we questioned whether repeated administration of the peptide OTUB2$_{58-66}$ could affect T1D onset in NOD mice. For this purpose, 6-week-old NOD mice were subcutaneously injected with the OTUB2$_{58-66}$ peptide mixed with poly IC (OTUB2$_{58-66}$) or with poly IC alone (Control) once a week for a total of three injections, and then the blood glucose level was measured weekly to monitor T1D onset (Fig. 6A). As expected, repeated administration of the OTUB2$_{58-66}$ peptide significantly reduced the incidence of T1D in NOD mice (Fig. 6B). Notably, when compared with that in control NOD mice injected with poly IC alone, the absolute number of pancreas-infiltrating lymphocytes in OTUB2$_{58-66}$-vaccinated NOD mice was increased significantly after 2 injections but significantly decreased after 3 injections (Fig. 6C). Additionally, the frequency of OTUB2$_{58-66}$ dextramer$^+$ CD8$^+$ T cells in pancreas-infiltrating lymphocytes in OTUB2$_{58-66}$-vaccinated NOD mice remained unchanged or even was increased slightly after 2 injections but was decreased after 3 injections when compared with that in control NOD mice (Fig. 6D, 6E). Consistently, three injections of OTUB2$_{58-66}$ reduced the production of IFN-γ and TNF-α by NOD mouse splenocytes upon PMA or OTUB2$_{58-66}$ stimulation (Fig. 6F, 6G).

We further speculated that repeated vaccination with the OTUB2$_{58-66}$ peptide might induce apoptosis or exhaustion in OTUB2$_{58-66}$-specific T cells and other diabetogenic T cells, thereby resulting in protection against T1D. As expected, the levels of Annexin V, FAS and PD-1 on the surface of OTUB2$_{58-66}$ Dextramer$^+$ CD8$^+$ T cells in pancreas-infiltrating lymphocytes in OTUB2$_{58-66}$-vaccinated NOD mice were much higher than those in control mice after 3 injections (Fig. S6A). In addition, the surface expression levels of Annexin V and FAS on CD3$^+$ CD8$^-$ T cells (mainly CD4$^+$ T cells) and CD3$^+$ CD8$^+$ T cells in the pancreas of NOD mice after 3 injections of the OTUB2$_{58-66}$ peptide were also increased significantly, while PD-1 expression was unchanged in CD3$^+$ CD8$^-$ T cells but significantly increased in CD3$^+$ CD8$^+$ T cells in the pancreas of OTUB2$_{58-66}$-vaccinated NOD mice compared with the corresponding cell populations in poly IC-treated control mice (Fig. S6B,6C). Collectively, these results indicate that repeated administration of the OTUB2$_{58-66}$ peptide prevents the development of T1D in NOD mice, possibly not only by hampering the response of OTUB2$_{58-66}$-specific CD8$^+$ T cells but also by inducing apoptosis or failure of other pathogenic T cells through unknown bystander effects.

Discussion

In this study, by comparative analysis of the landscape of the naturally presented MIP of NIT-1 β cells under steady- and ERS-state conditions, we identified the previously undescribed ERS-associated β cell

self-peptide OTUB2$_{58-66}$, which was exclusively present in the MIP of ER-stressed NIT-1 β cells but not that of nonstressed cells. OTUB2$_{58-66}$-specific CD8$^+$ T cells were present and diabetogenic in NOD mice. High glucose intake amplified OTUB2$_{58-66}$-specific CD8$^+$ T-cell responses in NOD mice. Notably, repeated vaccination with the OTUB2$_{58-66}$ peptide prevented T1D onset in NOD mice.

Recent evidence suggests that ERS in β cells may drive the generation of neoepitopes, which are likely not available for negative selection in the thymus. However, the conventional MHC-I peptides of β cells, which are newly induced by ERS and recognized by autoreactive CD8$^+$ T cells, have received less attention. Gonzalez-Duque *et al.* identified a catalog of HLA-I peptides, including conventional peptides, mRNA splicing products and fusion peptides presented by human β cells cultured with or without inflammatory cytokines. However, they did not focus on emerging β cell antigenic peptides induced by inflammatory cytokines (26). Here, we used HG and TG treatments to induce ERS in NIT-1 β cells and focused on exploring conventional MHC-I peptides induced by ERS in β cells and their diabetogenic effects. The NIT-1 β cell line is suggested to be a useful tool for understanding changes in primary islet β cells during T1D pathogenesis (27–29). Previous studies have demonstrated that HG or TG treatment can induce ERS in NIT-1 β cells, thereby enhancing the immunostimulatory potential of NIT-1 β cells for whole NOD splenocytes or diabetogenic CD4$^+$ T-cell clones (25, 30). Here, we demonstrate that both HG treatment and TG treatment significantly enhanced the visibility of NIT-1 β cells to splenic CD8$^+$ T cells from NOD mice, which appears to be achieved not by enhanced surface MHC-I expression but by changes in the composition of the MIP induced by ERS. In support of this, a small number of conventional peptides, which were exclusively present in the MIP of ER-stressed NIT-1 β cells, exhibited obvious immunogenicity to NOD mouse CD8$^+$ T cells. Among these peptides, OTUB2$_{58-66}$ was predicted to be a weak binder for H-2Kd but showed a strong ability to stimulate an immune response in almost all NOD mice between 5 and 13 weeks of age, which spanned both the prodrome and early stages of T1D (31). Inspiringly, NOD mouse splenocytes responded more frequently to OTUB2$_{58-66}$ than to IGRP$_{206–214}$, a major known β cell target of diabetogenic CD8$^+$ T cells in NOD mice. These data, together with dextramer staining and cell proliferation, killing and adoptive transfer assay results, suggest that OTUB2$_{58-66}$ is a novel immunodominant self-peptide recognized by autoreactive CD8$^+$ T cells in NOD mice. We speculate that OTUB2$_{58-66}$-autoreactive CD8$^+$ T cells may not undergo negative selection in NOD mice because the OTUB2$_{58-66}$ peptide was not identified in our previously established dataset of the immunopeptidome derived from the NOD mouse thymus (24). Dudek *et al.* sequenced the immunopeptidome of NIT-1 β cells under basal and inflammatory conditions (32). However, neither Dudek *et al.* nor our group identified any of the immunodominant diabetogenic CD8$^+$ T-cell epitopes previously reported in NOD mice, possibly due to the low abundance of these naturally MHC-I-presented peptides not meeting the LC/MS/MS detection sensitivity. Using a targeted MS–based approach for multiple-reaction monitoring, IGRP$_{206-214}$ remains undetectable on NIT-1 cells under basal conditions (1 copy/cell) but can be detected on IFN-γ-treated NIT-1 cells (25 copies/cell), which to some extent reflects the increased MHC-I presentation induced by IFN-γ (32). INSB$_{15-23}$, another important H2-Kd-restricted

β cell self-peptide recognized by diabetogenic $CD8^+$ T cells in NOD mice (33), was also not found in Dudek's study or our MIP datasets due to its poor binding with H2-Kd (NetMHC rank > 2%). Therefore, we presume that compared with $IGRP_{206-214}$ and $INSB_{15-23}$, $OTUB2_{58-66}$ can be naturally presented in high abundance by H-2Kd in ER-stressed β cells, making it more immunodominant and more easily recognized by autoreactive $CD8^+$ T cells in NOD mice.

The source protein OTUB2 is a kind of ubiquitin hydrolase whose main function is to remove the ubiquitination label on proteins to prevent protein degradation (34). Studies have shown that OTUB2 plays crucial roles in cancer and other human diseases. In many cases, OTUB2 acts as a tumor promoter in different types of human cancer (35, 36). However, it may also act as a tumor suppressor in some special cases (37). Although OTUB2 is a ubiquitously expressed protein that is preferentially expressed in the testis and brain, our immunohistochemical results indicate that OTUB2 is relatively highly expressed in pancreatic islets. The role of OTUB2 in islets remains largely unknown. Beck A. *et al.* reported that OTUB2 is a novel promoter of β cell survival through the inhibition of NF-κB signaling (38). We found that OTUB2 expression in β cells could be upregulated by HG or TG treatment and that this upregulation of OTUB2 could be almost eliminated by ERS inhibition, suggesting that ERS may be related to the upregulation of OTUB2, thus leading to the processing and presentation of $OTUB2_{58-66}$ in β cells. Consistent with our results, in the datasets reported by Dudek *et al.*, $OTUB2_{58-66}$ was detected only in the immunopeptidome of IFN-γ-treated NIT-1 cells, not in that of untreated NIT-1 cells (32), highlighting that various environmental factors that induce ERS may promote MHC-I presentation of the $OTUB2_{58-66}$ peptide in β cells. A previous study demonstrated that ERS is critical for the generation of a prevalent preproinsulin signal peptide-derived autoantigenic peptide by modulating ERAP1 expression (39). However, the underlying mechanism of ERS in the processing and presentation of the $OTUB2_{58-66}$ peptide remains unknown.

Finally, we evaluated the potential use of the $OTUB2_{58-66}$ peptide for T1D prevention in NOD mice. Antigen-specific immune tolerance in T1D can be achieved by inducing antigen-specific regulatory cell populations, depleting diabetogenic T-cell clones, or inducing autoreactive T-cell anergy (40). Repeated antigen stimulation can effectively induce death in activated T cells, which is a favored goal for inducing immune tolerance because it achieves actual elimination of pathogenic T cells (41). Therefore, to effectively delete $OTUB2_{58-66}$-reactive $CD8^+$ T cells, we treated NOD mice with repeated subcutaneous injections of the $OTUB2_{58-66}$ peptide combined with poly IC, which is characterized to favor the activation and expansion of $CD8^+$ T cells (42). As expected, multiple immunizations with the $OTUB2_{58-66}$ peptide plus poly IC induced significant T1D protection in NOD mice. Surprisingly, this protective effect was accompanied not only by weakening of $OTUB2_{58-66}$-reactive $CD8^+$ T cells but also by an overall decline in pancreas-infiltrating T cells, manifested by a decreased infiltrating cell number and reduced proinflammatory cytokine production, as well as increased FAS, Annexin V, and PD-1 expression. We previously reported that repeated treatment with an altered peptide ligand of an HLA-A*0201-restricted insulin epitope could induce extensive suppressive bystander effects by inducing $CD8^+$ Tregs in

humanized NOD mice (43). Thus, we hypothesized that $OTUB2_{58-66}$ peptide immunization may exert extensive inhibitory bystander effects through a similar mechanism, which needs further study.

In summary, our findings suggest that environmental factors, such as a high-sugar diet, can trigger ERS in β cells, which induces β cells to process and present certain autoantigenic peptides, such as $OTUB2_{58-66}$, thereby increasing the visibility of β cells to the immune system and accelerating the progression of T1D in NOD mice. This study provided not only a new explanation for the role of ERS in promoting β cell-targeted autoimmunity but also a potential target for the prevention and treatment of T1D.

Limitations of the study

A limitation of this study is that we ignored potential ERS-induced unconventional peptides, as their accurate identification remains a great challenge. There are some differences between the NIT-1 β cell line and primary NOD islet β cells. Although the presence of $OTUB2_{58-66}$-specific $CD8^+$ T cells in NOD mice has been confirmed, whether the $OTUB2_{58-66}$ peptide can be naturally presented by MHC-I molecules on the surface of primary β cells under ERS remains to be confirmed. Most autoantigens identified in NOD mice have also been shown to be targets of T-cell-mediated autoimmunity in human T1D, but whether OTUB2 is a human T1D autoantigen requires further investigation.

METHODS

Antibodies and reagents

The antibodies against the following proteins/epitopes were purchased from the indicated sources: Mouse CD4, Biotin (eBioscience, cat.no.13-0041-85), Mouse H-2 (Bioxcell, cat.no. BE0077), Mouse H-2Kd (Bioxcell, cat.no.BE0104), Mouse TXNIP (Cell signaling, cat.no.14715), Mouse ATF6 (Cell Signaling, cat. no.65880s), Mouse XBP-1(Abcam, cat. no.ab220783), Mouse XBP-1s (Cell Signaling, cat. no. 40435), Mouse eIF2a (Cell signaling, cat. no. 2103), Mouse eIF2a-P (Cell signaling, cat.no. 9721); Mouse IRE1 (Thermo fisher, cat.no.PA1-16928), Mouse IRE1-P (Thermo fisher, cat.no.PA1-16927), Mouse α-tubulin (Beyotime, cat.no.AF0001), Mouse TNF-α-APC (BioLegend, cat.no. 506308), Mouse IFN gamma-PE (BioLegend, cat.no.505808), Mouse CD3-APC-Cy7 (BioLegend, cat.no.100222), Mouse CD44-PerCP-Cy5.5 (BioLegend, cat.no.103032), Mouse CD62L-PE-Cy7 (BD, cat.no.560516), Mouse CD8-PE-Cy7 (BioLegend, cat. no.126616), Mouse CD3-Percy-Cy5.5 (BioLegend, cat.no.100218), Mouse H-2Kd-APC (Invitrogen, cat.no.116620), Mouse CD4-FITC (BioLegend, cat.no.100406), Mouse CD3-BV421 (BioLegend, cat.no. 100228), Mouse CD11c-FITC (BioLegend, cat.no.117306), Mouse I-A/I-E-PE (BioLegend, cat.no.107608), Mouse CD80-PerCP-Cy5.5 (BioLegend, cat.no.104722), Mouse CD8a-BV510 (BioLegend, cat.no.126631), Mouse OTUB2 (Assay Genie, cat.no. PACO 01270), Mouse Insulin (Abcam, cat.no. ab7842), Mouse CD8(Abcam, cat.no. ab217344), Guinea Pig IgG H&L-Alexa Fluor® 647 (Abcam, cat.no. ab150187), Rabbit IgG(H + L)-Cy3 (Beyotime, cat.no. A0516), Mouse CD95 (Fas)-FITC (BioLegend, cat.no. 152605), Mouse PD-1-BV421 (BioLegend, cat.no. 135217).

The following reagents were purchased from the indicated companies: ELISPOT specific serum-free medium (DAKEWE, cat.no.6015012), BeaverBeads™ Streptavidin (BEAVER, cat.no. 22307-10), RPMI 1640 Medium, GlutaMAX™ (Gibco, cat.no.61870-036), MEM Nonessential Amino Acids (Corning, cat.no.25-025-CI), Sodium pyruvate (Gibco, cat.no.11360-070), L-Glu (Gibco, cat.no.25030-081), Recombinant Murine GM-CSF (Peprotech, cat.no.315-03), Recombinant Murine IL-4 (Peprotech, cat.no.214 – 14), Murine IL-2 (Poprotech, cat.no. 212 – 12), Lipopolysaccharide (Sigma, cat.no. L4391), PrimeScrep RT reagent kit (TAKARA, cat.no. RR037A), TB Green Premix EX TaqTM II (TAKARA, cat.no. RR820A), NuPAGE 4%-12% Bis-Tris Gel (Invitrogen, cat.no.NP033BOX), Pre-stained Color Protein Ladder (Beyotime, cat.no. P0079), NuPAGE™ MOPS SDS Running Buffer (Thermo fisher, cat.no. NP0001), HiTrap NHS-activated HP (GE health, cat.no.17-0716-01), Ham's F-12K (Kaighn's) Medium (Gibco, cat.no.21127022), TG (Abcam, cat.no. ab120286), Glucose (Sigma, cat.no. G8270), Dextramer-PE (Immudex), Glucose (Rhawn, cat.no. R049603), Collagenase IV (Sigma, cat.no.C5138), DNase I (Roche, cat.no.11284932001), Mouse lymphocyte isolation solution (DAKEWE, cat.no. 7211011), PMA (Abcam, cat.no. ab120297), Ionomycin (Sigma, cat.no. I9657), GolgiStop (BD, cat.no. 554724), Poly IC (InvivoGen, cat.no. vac-pic), Sanuo blood glucose test paper (Cell biological, cat.no. CELLXTSZ-600), APC Annexin V (Biolegend, cat.no. 640920), Annexin V Binding Buffer (Biolegend, cat.no. 422201), Mouse IFN-γ ELISPOT kit (Dakewei, cat.no. 2210006), Mouse $CD8^+$ T cell enrichment kit (StemCell Technologies, cat.no.19853), Intracellular Fix & Perm Buffer set (eBiosciences, cat.no. 88-8824), Count Bright Plus Absolute Counting Beads (Scientific Thermo Fisher, cat.no. C36995), BCA Protein Assay Kit (Beyotime, cat.no. P0012), CFSE Cell Proliferation Kit (Invitrogen, cat.no. C34554).

Primers

The following primers were synthesized by Sangon Biotech (Shanghai, China): GAPDH (Forward: CGTCCCGTAGACAAAATGGT; Reverse: GAATTTGCCGTGAGTGGAGT), XBP-1s (Forward: CTGAGTCCGAATCAGGTGCAG; Reverse: GTCCATGGGAAGATGTT CTGG), CHOP (Forward: CTGGAAGCCTGGTATGAGGAT; Reverse: CAGGGTCAAGAG TAGTGAAGGT), TXNIP (Forward: GGCCGGACGGGTAATAGTG; Reverse: AGCGCAA GTAGTCCAAAGTCT), ATF6 (Forward: TCGCCTTTTAGTCCGGTTCTT; Reverse: GGCT CCATAGGTCTGACTCC), eIF2α (Forward: CACCGCTGTTGACAGTCAGAG; Reverse: GCAAACAATGTCCCATCCTTACT), Otub2 (Forward: AACTCAGCAAAAGATTCACCTC G; Reverse TCATTTGGGGTCTGTAGCACA).

NIT-1 Cell Culture

The pancreatic β-cell line NIT-1 was maintained in F-12K (Gibco, US) complete medium containing 10% fetal bovine serum (FBS) under 5% CO2 at 37°C. For HG and TG pretreatments, cells were cultured with 10 mM, 20 mM or 30 mM HG for 24 h or 48 h or cultured with 1 μM, 5 μM or 10 μM TG for 0.5 h or 1 h and then washed extensively with PBS. Then, 1×10^4 cells were collected for mouse IFN-γ ELISPOT assays.

IFN-γ ELISPOT Assays

$CD4^-$ T cells were isolated from freshly prepared single-cell suspensions of NOD mouse splenocytes by using BeaverBeads™ Meg streptavidin (Beaver Biosciences Inc., Guangzhou, China) and a biotinylated anti-CD4 antibody (clone: GK1.5 Invitrogen). A total of 1×10^5 remaining $CD4^-$ splenocytes and 1×10^4 NIT-1 cells treated with or without different concentrations of glucose or TG for different times were cultured in 96-well ELISPOT plates precoated with a specific capture antibody against IFN-γ (Dakewei Biotech, Shenzhen, China) at 37°C and 5% CO2 for 20 h. To block the H-2Kd-restricted recognition of $CD8^+$ T cells, NIT-1 cells treated with 20 mM glucose for 24 h or 5 μM TG for 0.5 h were preincubated with an anti-H-2Kd antibody (SF1.1.10, 50 μg/ml) for 2 h and then cocultured with $CD4^-$ splenocytes. After the incubation, the cells were removed, and the plates were processed according to the ELISPOT kit manufacturer's instructions. Spots were counted using a spot reader system (Saizhi, Beijing, China).

Western Blot and Quantitative Reverse Transcription (qRT)-PCR Analyses

NIT-1 cells were treated with or without 20 mM glucose for 24 h or 5 μM TG for 0.5 h, and then cell samples were collected at 0 h, 6 h, 12 h and 24 h after withdrawal of HG or TG treatment. For the western blot assay, cell samples were lysed with RIPA lysis buffer (Beyotime) containing 1 mM PMSF (Beyotime). The proteins in the lysates were separated by SDS-PAGE and immunoblotted with the following primary antibodies: mouse anti-eIF2a (2103, Cell Signaling), rabbit anti-eIF2a-P (9721, Cell Signaling), rabbit anti-XBP-1 (ab220783, Abcam), rabbit anti-XBP-1s (40435, Cell Signaling), rabbit anti-ATF6 (65880s, Cell Signaling), rabbit anti-TXNIP (D5F3E) (14715, Cell Signaling), rabbit anti-IRE1 (PA1-16928, Thermo Fisher), rabbit anti-IRE1-P (PA1-16927, Thermo Fisher) and rabbit anti-α-tubulin (AF0001, Beyotime). After an incubation with peroxidase-coupled secondary antibodies for 60 min, the immunocomplexes were visualized using a chemiluminescence reagent (Amersham, Freiburg, Germany), and the autoradiographs were scanned by an imaging densitometer. For qRT-PCR, total RNA was isolated from cell samples using TRIzol reagent (Invitrogen,US). Total RNA (500 ng) was reverse transcribed into cDNA using the PrimeScript® RT Reagent Kit (TaKaRa, Japan). Real-time quantitative PCR was performed using TB Green™ Premix Ex Taq™ II (Tli RNaseH Plus) (Takara, Japan) to detect the relative expression of TXNIP, CHOP, XBP-1s, ATF6 and eIF2a. Each sample run was performed in triplicate, and relative mRNA expression levels were determined using the 2(-Delta Ct) method with Gapdh as the internal reference control.

Isolation of the MIP of NIT-1 cells

A total of 5×10^8 untreated NIT-1 cells (NC group), NIT-1 cells treated with 20 mM glucose for 24 h and cultured for another 24 h after treatment withdrawal (HG group) or NIT-1 cells treated with 5 μM TG for 0.5 h and cultured for another 12 h after treatment withdrawal (TG group) were harvested and immediately lysed in 20 ml of ice-cold lysis buffer (50 mM Tris pH 8.0, 150 mM NaCl, and 1% CHAPS) containing a "complete" protease inhibitor (Roche). The cell lysates were clarified by centrifugation at 4°C and 17000 rpm for 30 min, which was repeated 3 times, and the clean supernatant was filtered through a 0.2-μm needle filter (Thermo Fisher) and collected. The procedure used for the isolation of the

MIP was performed according to our previously reported method (24). Briefly, according to the manufacturer's instructions for an HP column, immunoaffinity columns were constructed by using a 1-mL HiTrap NHS-activated HP column (Code No:17-0716-01, GE Healthcare) coupled with 10 mg anti-H-2 mAb (clone: M1/42.3.9.8, BioXCell). The NIT-1 cell proteolytic solution was repeatedly circulated in the column overnight at a flow rate of 0.5 mL/min at 4°C. Then, the column was washed with several buffers in the following order: 50 mM Tris (pH 8.0), 150 mM NaCl and 1% CHAPS; 50 mM Tris-HCl (pH 8.0) and 150 mM NaCl; 50 mM Tris-HCl (pH 8.0) and 450 mM NaCl; and 50 mM Tris-HCl (pH 8.0). Subsequently, the MHC I-peptide complexes were eluted with 4 mL of 10% acetic acid. Ultrafiltration filters (3.0-kDa cutoff Microcon, Millipore) were prewashed with double-distilled water three times and 10% acetic acid one time to remove contaminants interfering with MS. Then, the mixture of peptides, the class I heavy chain and β2-microglobulin was separated by ultrafiltration at 8500 × g for 30 min at 4°C. After ultrafiltration, the peptide mixture was desalinated and concentrated on a Micro-Tip reversed-phase C18 column (Merck)(44).

LC-MS/MS analysis of the MIP of NIT-1 cells

Desalted peptides were dissolved in solvent A (0.1% formic acid, 2% acetonitrile) and directly loaded onto a reversed-phase analytical column (25-cm length, 100 μm i.d.) made in-house. The peptides were separated with a gradient from 4–23% solvent B (0.1% formic acid in 90% acetonitrile) over 62 min, 23–35% over 20 min, climbing to 80% over 4 min and then holding at 80% for the last 4 min, all at a constant flow rate of 450 nL/min, on an EASY-nLC 1200 UPLC system (Thermo Fisher Scientific).

The separated peptides were analyzed in a Q Exactive™ HF-X (Thermo Fisher Scientific) with a nanoelectrospray ion source. The electrospray voltage applied was 2.2 kV. The full MS scan resolution was set to 120,000 for a scan range of 400–1500 m/z. Up to 10 of the most abundant precursors were then selected for further MS/MS analyses with 30-s dynamic exclusion. HCD fragmentation was performed at a normalized collision energy (NCE) of 28%. The fragments were detected in the Orbitrap at a resolution of 45,000. The automatic gain control (AGC) target was set at 5E4, with an intensity threshold of 1E4 and a maximum injection time of 40 ms. Samples were analyzed in three technical replicates and two biological replicates. The mass spectrometry proteomics data have been deposited to the ProteomeXchange Consortium via the PRIDE [1] partner repository with the dataset identifier PXD041227.

Mass spectrometry data analysis of the MIP

All tandem mass spectra were queried against a custom MHC class I-targeted database we previously established (24), using the MaxQuant (version 1.5.2.8), Sequest and Mascot (implemented with Proteome Discoverer 2.1) search engines with no cleavage restriction. For all searches, the parent mass error tolerance was set to 10 ppm and the fragment mass error tolerance to 0.02 Da. Oxidation of methionine was considered a variable modification. The confidence peptides were filtered at a 5% false discovery rate (FDR) at the peptide-spectrum match (PSM) level. According to the literature (45), to integrate the advantages of multiple search algorithms and identify more possible peptides, the

MaxQuant, Mascot and Sequest search results in technical triplicates and biological duplicates were combined to establish the datasets MIP of the NIT-1 cells.

Determination of MHC class I motifs

The logo program (http://weblogo.berkeley.edu/logo.cgi?tdsourcetag=s_pctim_aiomsg) was used to visualize the characteristics of peptide-binding motifs. The information content at each position in the sequence motif was indicated using the height of a column of letters, representing amino acids. The height of each letter within the columns was proportional to the frequency of the corresponding amino acid at that position.

Peptide synthesis

Peptides were synthesized at the Chinese Peptide Company (Hangzhou, China) with a purity of over 95%. The synthetic peptides were identified by LC-MS/MS with the parameter settings used for MIP identification.

Generation of NOD mouse bone marrow-derived dendritic cells (BMDCs)

NOD mouse bone marrow-derived dendritic cells (BMDCs) were generated according to a previously reported protocol (46). Briefly, NOD mouse bone marrow cells were cultured in the presence of 20 ng/mL granulocyte-macrophage colony-stimulating factor (GM-CSF) and 10 ng/mL interleukin-4 (IL-4) for 6 days. To induce further maturation, DCs were recultured in the presence of 1 μg/mL lipopolysaccharide (LPS, Sigma) for an additional 24 h. To evaluate the purity and maturity of cultured DCs, cells cultured for 7 days were harvested and stained with the fixable viability dye eFluor® 780 (eBioscience), BV421-conjugated anti-mouse CD3, FITC-conjugated anti-mouse CD11C, PE-conjugated anti-mouse MHC II, and PerCP-Cy5.5-conjugated anti-mouse CD80 for 20 min at 4°C in the dark. After washing, the samples were detected on a BD FACSCalibur (BD Biosciences, Franklin Lakes, NJ), and the data were analyzed using FlowJo V10 software.

Immunogenicity evaluation of candidate peptides

Freshly prepared $CD4^-$ NOD mouse splenocytes were primed with each candidate peptide (50 μg/mL) in the presence of 50 U/mL recombinant murine interleukin 2 (rmIL-2, PeproTech, Rocky Hill, NJ, USA). On Day 7, the peptide-primed $CD4^-$ splenocytes (2×10^5 cells/well) were cocultured with peptide (50 μg/mL)-pulsed DCs (1×10^4 cells/well) in 96-well ELISPOT plates precoated with a specific capture antibody against IFN-γ (Dakewei Biotech, Shenzhen, China) at 37°C and 5% CO2 for 20 h. After the incubation, the cells were removed, and the plates were processed according to the ELISPOT kit manufacturer's instructions. Spots were counted using a spot reader system (Saizhi, Beijing, China).

Isolation of pancreas-infiltrating lymphocytes from NOD mice

Pancreas-infiltrating lymphocytes were isolated according to the protocol of a previous report with some modifications (47). Briefly, after removing all visible pancreatic lymph nodes, the pancreas was digested in 3 ml HBSS containing 1 mg/mL collagenase IV (Sigma) and 0.02 mg/mL DNase I with stirring (200 rpm) for 15 min in a 5% CO2 cell incubator at 37°C. The single-cell suspensions were collected after diluting the enzyme mixture with 3 mL ice-cold HBSS containing 5% FBS and removal of the aggregates by settling for 2 min on ice. The aggregates were further digested with 3 mL half collagenase IV and DNase I for 10 min. The single-cell suspensions were washed two times with HBSS containing 5% FBS and then resuspended in 2 ml RPMI 1640 medium containing 5% FBS. Two milliliters of cell suspension was laid on the surface of 2 mL mouse lymphocyte separation medium (DAKEWE) slowly and carefully to form a clear boundary. After 1800 r/min centrifugation for 20 minutes, the lymphocytes were carefully collected and washed twice with 5 ml PBS containing 5% FBS.

Dextramer staining

Lymphocytes isolated from the spleen, pancreas and pancreas-draining lymph nodes of NOD mice suspended in PBS containing 5% FBS (2×10^6 cells/50 μL) were initially stained with PE-conjugated dextramer (10 μL/test) in the dark at room temperature for 10 min and then stained with Fixable Viability Dye eFluor® 780 (eBioscience), FITC-conjugated anti-CD3, BV510-conjugated anti-CD8, BV421-conjugated anti-CD107, PerCP-Cy5.5-conjugated anti-CD44, and PE-Cy7-conjugated anti-CD62L in the dark at 2–8°C for 20 min. The cells were washed twice with 2 ml PBS/5% FBS and immediately analyzed on a BD FACSCalibur (BD Biosciences, Franklin Lakes, NJ).

Intracellular cytokine staining of $CD8^+$ T cells

Splenocytes isolated from NOD mice were stimulated with or without peptide (50 μg/mL) or PMA in complete medium containing 0.65 μl/mL GolgiStop™ (BD Biosciences) for 4 h. Dead cells were excluded from the analysis by using the fixable viability dye eFluor® 780 (eBioscience). PerCP-Cy5.5-conjugated anti-CD3 (17A2, BioLegend) and PE-Cy7-conjugated anti-CD8 (53 – 6.7, BioLegend) were used to label the cells for 30 min on ice. After washing with flow cytometry buffer (PBS/1% FBS), the cells were fixed and then labeled with APC-conjugated anti-mouse TNF-α (MP6-XT22, BioLegend) and PE-conjugated anti-mouse IFN-γ (XMG1.2, BioLegend) at 4°C in permeabilization buffer. Data were acquired for each of the experiments using a BD FACSCalibur (BD Biosciences, Franklin Lakes, NJ). Data analysis was performed using FlowJo software.

CFSE-based $CD8^+$ T-cell proliferation assay

$CD4^-$ T-cells freshly isolated from NOD mice splenocytes were stained with 0.5 μM carboxyfluorescein succinimidyl ester (CFSE; Invitrogen). After extensive washing, the CFSE-labeled splenocytes were cocultured with or without 10 μg/mL peptide in the presence of 50 U/mL rmIL-2 on Day 1. Half of the medium was replaced every 3 days and supplemented with rmIL-2. On Day 6, the cultured cells were harvested and stained with the fixable viability dye eFluor® 780 (eBioscience) and PE-Cy7-conjugated anti-mouse CD8 (YTS156.7.7, BioLegend). Then, the cell samples were washed twice with PBS and

analyzed on a BD FACSCalibur (BD Biosciences, Franklin Lakes, NJ), and the data were analyzed using FlowJo V10 software.

CFSE-based cytotoxicity assay

A CFSE-based cytotoxicity assay was performed according to a previously reported protocol (48). Briefly, after washing with PBS, NOD mouse splenocytes were resuspended at 2×10^7 cells/mL and labeled with 10 μM CFSE (Invitrogen), after two washes, the CFSE-labeled splenocytes were incubated with or without peptide (50 μg/mL) at 37°C and 5% CO2 for 2 h. After another 2 washes, the cell concentration was adjusted to 1×10^5 cells/mL, and cells were seeded in 96-well microtiter plates at 100 μL/well as target cells. $CD8^+$ T cells were enriched from NOD mouse splenocytes using a mouse $CD8^+$ T-cell enrichment kit (StemCell Technologies), and the cell concentration was adjusted to 1×10^7 cells/mL. $CD8^+$ T cells were seeded in the 96-well microtiter plates at 100 μL/well as effector cells, and the effector-target ratio was 100:1. After an incubation at 37°C in 5% CO2 for 5 h, the cells were stained with the fixable viability dye eFluor® 780 for 20 min at 4°C in the dark to stain dead cells, washed with PBS and resuspended in 300 μL PBS/test. The cell samples were mixed with 10000 Flow-Count Fluorospheres (Coulter Corporation, Miami, FL) and analyzed by flow cytometry. A total of 5000 microbeads were acquired for each sample, and the absolute number of surviving cells was determined by calculating the ratio between the number of cells and the number of beads. The percentage of viability cells was calculated as follows: % survival= [absolute no. viable $CFSE^+$ target cells (t = x)]/[absolute no. viable $CFSE^+$ target cells (t = 0)]×100.

$OTUB2_{58-66}$-specific $CD8^+$ T-cell proliferation and adoptive transfer

Six-week-old NOD mice were randomly divided into two groups and then subcutaneously injected with 30 μg $OTUB2_{58-66}$ mixed with 30 μg poly IC ($OTUB2_{58-66}$ group) or 30 μg poly IC alone (control group) in 100 μL PBS, with one injection administered per week for two weeks. Splenocytes isolated from the immunized NOD mice were stimulated with or without $OTUB2_{58-66}$ peptides (50 ng/mL) for one week and maintained in 50 U/mL IL-2 in vitro. After three washes with PBS, the cells were resuspended in 2 ml PBS and injected into NOD/scid mice via the tail vein at 1×10^7/200 μL/mouse. The blood glucose level of NOD/scid mice was measured 4 weeks after the transfusion to detect the onset of T1D. After disease onset or at the end of the experimental observation period, pancreatic tissue was taken for hematoxylin and eosin (H&E) staining to detect insulitis. A minimum of 10 islets from each mouse were microscopically observed by two different observers, and insulitis scoring was performed according to the following criteria: 0, no infiltration; 1, peri-insulitis; 2, insulitis with < 50% islet area infiltrated; and 3, insulitis with > 50% islet area infiltrated. Laser confocal microscopy imaging of CD8 and insulin was performed to detect the infiltration of $CD8^+$ T cells in pancreatic islets. Briefly, pancreas paraffin sections were incubated with a guinea pig anti-insulin antibody (Abcam ab7842) and rabbit anti-CD8 alpha antibody (Abcam ab217344, EPR21769) at 4°C overnight. The samples were then incubated with goat

anti-guinea pig IgG H&L (Alexa Fluor® 647, ab150187) and Cy3-labeled goat anti-rabbit IgG H&L (Alexa Fluor® 555, Beyotime A0516) for 1 h, and then the nuclei were stained with DAPI for 0.5 h. The stained samples were observed using a confocal laser scanning microscope (Zeiss LSM780NLO).

OTUB2 expression in NIT-1 cells and the pancreas of NOD mice

Total RNA and protein samples were extracted from NIT-1 cells (NIT-1-NC), NIT-1 cells treated with 20 mM HG for 24 h (NIT-1-HG) and NIT-1 cells treated with 5 μM TG for 0.5 h (NIT-1-TG). Relative OTUB2 mRNA levels were determined by real-time qRT-PCR, and each sample run was performed in triplicate and evaluated using the $2^{(-\triangle\triangle Ct)}$ method (49) with Gapdh as the internal reference control. For the western blot assay, total protein samples were separated by SDS-PAGE and transferred to a PVDF membrane by electroblotting (50). The expression levels of OTUB2 in NIT-1 cells and the NOD mouse pancreas were determined using enhanced chemiluminescence. Immunohistochemical analysis of OTUB2 expression in the NOD mouse pancreas was carried out as described (49).

Mouse treatment

Female NOD mice, NOD/scid mice and ICR mice (HFK Bioscience, Beijing, China) were maintained under a 12-h light/dark cycle in specific pathogen-free facilities and allowed free access to sterilized water and food. All procedures were approved by the Institute Animal Care and Use Committee of Army Medical University (Chongqing, China).

Four-week-old female NOD mice were randomly divided into two groups given normal water (NC group) or 20% glucose water (HG group). The mice were sacrificed at the age of 6 or 12 weeks, and lymphocytes were isolated from the spleen and pancreas for flow cytometry analysis.

Six-week-old female NOD mice were randomly divided into two groups and then subcutaneously injected with 30 μg $OTUB2_{58-66}$ plus 30 μg poly IC ($OTUB2_{58-66}$ group) or 30 μg poly IC alone (control group) dissolved in 100 μL PBS once per week for three consecutive weeks. After three injections, blood glucose levels were measured weekly until disease onset or the end of the experimental observation period (25 weeks). NOD mice were sacrificed after 2 or 3 injections, and lymphocytes were isolated from the spleen and pancreas for flow cytometry analysis.

Statistical analysis

Prism5 software (GraphPad Software) was used for all statistical analyses. The survival curves of two groups were compared by the log-rank (Mantel–Cox) test, and unpaired two-group comparisons were conducted using Student's t test. Data are presented as the mean ± SD. $P < 0.05$ (*), $P < 0.01$ (**) and $P < 0.001$ (***) were considered statistically significant.

Data availability

All data that support the findings of this study are available within source data and supplementary information files. The mass spectrometry proteomics raw data have been deposited to the ProteomeXchange Consortium via the PRIDE [1] partner repository with the dataset identifier PXD041227.

Declarations

Data availability

All data that support the findings of this study are available within source data and supplementary information files. The mass spectrometry proteomics raw data have been deposited to the ProteomeXchange Consortium via the PRIDE [1] partner repository with the dataset identifier PXD041227.

Acknowledgments

This work was supported by National Natural Science Foundation of China (No. 81871301 and No. 82071825) and National Key Research and Development Program (No. 2016YFA0502204). We also thanks Quan Zhou, Mingfu Ye and Xiaojun Peng (PTM-biolabs, China) for assistance with MS data analysis.

Author contributions

LW performed main experiments and draft the manuscript. JL and XL performed flow cytometry staining and analysis, GM and ZZ performed the HE staining of pancreas paraffin section, XC and SY performed immunohistochemistry, MZ prepared the biological samples and isolated MHC I-peptides complexes, JZ and SW analyzed MS data. LW planned the experiments, interpreted the results, evaluated the data and completed the manuscript. YW supervised and managed the research process, completed the manuscript and provided research funds. All authors contributed to the article and approved the submitted version.

COMPETING INTERESTS

The authors declare no competing interests.

ETHICS APPROVAL AND CONSENT TO PARTICIPATE

This study was approved by the Ethics Committee of the Army Medical University (Third Military Medical University).

Additional information

Supplementary figure legends

Supplementary figures

Table S1: Total peptides in the MIP of NIT-1 cells

Table S2: Unique peptides in the ER-stressed NIT-1 MIP

Lead contact

Further information and requests for resources and reagents should be directed to and will be fulfilled by the lead contact, Li Wang (Email:liwang118@tmmu.edu.cn).

References

1. Norris JM, Johnson RK, Stene LC. Type 1 diabetes-early life origins and changing epidemiology. The Lancet Diabetes & Endocrinology. 2020;8(3):226–38.
2. von Scholten BJ, Kreiner FF, Gough SCL, von Herrath M. Current and future therapies for type 1 diabetes. Diabetologia. 2021;64(5):1037–48.
3. Pugliese A. Autoreactive T cells in type 1 diabetes. The Journal of clinical investigation. 2017;127(8):2881–91.
4. Culina S, Lalanne AI, Afonso G, Cerosaletti K, Pinto S, Sebastiani G, et al. Islet-reactive CD8(+) T cell frequencies in the pancreas, but not in blood, distinguish type 1 diabetic patients from healthy donors. Science immunology. 2018;3(20).
5. Wang J, Tsai S, Shameli A, Yamanouchi J, Alkemade G, Santamaria P. In situ recognition of autoantigen as an essential gatekeeper in autoimmune CD8 + T cell inflammation. Proceedings of the National Academy of Sciences of the United States of America. 2010;107(20):9317–22.
6. Noble JA, Valdes AM, Varney MD, Carlson JA, Moonsamy P, Fear AL, et al. HLA class I and genetic susceptibility to type 1 diabetes: results from the Type 1 Diabetes Genetics Consortium. Diabetes. 2010;59(11):2972–9.
7. Yoneda R, Yokono K, Nagata M, Tominaga Y, Moriyama H, Tsukamoto K, et al. CD8 cytotoxic T-cell clone rapidly transfers autoimmune diabetes in very young NOD and MHC class I-compatible scid mice. Diabetologia. 1997;40(9):1044–52.
8. de Verteuil D, Granados DP, Thibault P, Perreault C. Origin and plasticity of MHC I-associated self peptides. Autoimmunity reviews. 2012;11(9):627–35.
9. Perreault C. The origin and role of MHC class I-associated self-peptides. Progress in molecular biology and translational science. 2010;92:41–60.
10. So JS. Roles of Endoplasmic Reticulum Stress in Immune Responses. Molecules and cells. 2018;41(8):705–16.
11. Liu H, Wang H, Chen D, Gu C, Huang J, Mi K. Endoplasmic reticulum stress inhibits 3D Matrigel-induced vasculogenic mimicry of breast cancer cells via TGF-beta1/Smad2/3 and beta-catenin signaling. FEBS open bio. 2021;11(9):2607–18.

12. Yong J, Johnson JD, Arvan P, Han J, Kaufman RJ. Therapeutic opportunities for pancreatic beta-cell ER stress in diabetes mellitus. Nature reviews Endocrinology. 2021;17(8):455–67.
13. Eizirik DL, Cardozo AK, Cnop M. The role for endoplasmic reticulum stress in diabetes mellitus. Endocrine reviews. 2008;29(1):42–61.
14. Horwitz MS, Ilic A, Fine C, Balasa B, Sarvetnick N. Coxsackieviral-mediated diabetes: induction requires antigen-presenting cells and is accompanied by phagocytosis of beta cells. Clinical immunology. 2004;110(2):134–44.
15. Like AA, Rossini AA. Streptozotocin-induced pancreatic insulitis: new model of diabetes mellitus. Science. 1976;193(4251):415–7.
16. Delmastro MM, Piganelli JD. Oxidative stress and redox modulation potential in type 1 diabetes. Clinical & developmental immunology. 2011;2011:593863.
17. Karunakaran U, Elumalai S, Moon JS, Jeon JH, Kim ND, Park KG, et al. Myricetin Protects Against High Glucose-Induced beta-Cell Apoptosis by Attenuating Endoplasmic Reticulum Stress via Inactivation of Cyclin-Dependent Kinase 5. Diabetes & metabolism journal. 2019;43(2):192–205.
18. Jiang Z, Woda BA. Cytokine gene expression in the islets of the diabetic Biobreeding/Worcester rat. Journal of immunology. 1991;146(9):2990–4.
19. Lamb MM, Frederiksen B, Seifert JA, Kroehl M, Rewers M, Norris JM. Sugar intake is associated with progression from islet autoimmunity to type 1 diabetes: the Diabetes Autoimmunity Study in the Young. Diabetologia. 2015;58(9):2027–34.
20. Li X, Wang L, Meng G, Chen X, Yang S, Zhang M, et al. Sustained high glucose intake accelerates type 1 diabetes in NOD mice. Frontiers in Endocrinology. 2022;13.
21. Marre ML, Profozich JL, Coneybeer JT, Geng X, Bertera S, Ford MJ, et al. Inherent ER stress in pancreatic islet beta cells causes self-recognition by autoreactive T cells in type 1 diabetes. Journal of autoimmunity. 2016;72:33–46.
22. Kracht MJ, van Lummel M, Nikolic T, Joosten AM, Laban S, van der Slik AR, et al. Autoimmunity against a defective ribosomal insulin gene product in type 1 diabetes. Nature medicine. 2017;23(4):501–7.
23. Delong T, Wiles TA, Baker RL, Bradley B, Barbour G, Reisdorph R, et al. Pathogenic CD4 T cells in type 1 diabetes recognize epitopes formed by peptide fusion. Science. 2016;351(6274):711–4.
24. Wang L, Li X, Yang S, Chen X, Li J, Wang S, et al. Proteomic identification of MHC class I-associated peptidome derived from non-obese diabetic mouse thymus and pancreas. Journal of proteomics. 2023;270:104746.
25. Li X, Wang L, Meng G, Chen X, Yang S, Zhang M, et al. Sustained high glucose intake accelerates type 1 diabetes in NOD mice. Front Endocrinol (Lausanne). 2022;13:1037822.
26. Gonzalez-Duque S, Azoury ME, Colli ML, Afonso G, Turatsinze JV, Nigi L, et al. Conventional and Neo-antigenic Peptides Presented by beta Cells Are Targeted by Circulating Naive CD8 + T Cells in Type 1 Diabetic and Healthy Donors. Cell metabolism. 2018;28(6):946–60 e6.

27. Hamaguchi K, Gaskins HR, Leiter EH. NIT-1, a pancreatic beta-cell line established from a transgenic NOD/Lt mouse. Diabetes. 1991;40(7):842–9.
28. Wen X, Zhu H, Li L, Li Y, Wang M, Liu J, et al. Transplantation of NIT-1 cells expressing pD-L1 for treatment of streptozotocin-induced diabetes. Transplantation. 2008;86(11):1596–602.
29. Stephens LA, Thomas HE, Kay TW. Protection of NIT-1 pancreatic beta-cells from immune attack by inhibition of NF-kappaB. Journal of autoimmunity. 1997;10(3):293–8.
30. Marré ML, Piganelli JD. Environmental Factors Contribute to β Cell Endoplasmic Reticulum Stress and Neo-Antigen Formation in Type 1 Diabetes. Front Endocrinol (Lausanne). 2017;8:262.
31. Andre I, Gonzalez A, Wang B, Katz J, Benoist C, Mathis D. Checkpoints in the progression of autoimmune disease: lessons from diabetes models. Proceedings of the National Academy of Sciences of the United States of America. 1996;93(6):2260–3.
32. Dudek NL, Tan CT, Gorasia DG, Croft NP, Illing PT, Purcell AW. Constitutive and inflammatory immunopeptidome of pancreatic beta-cells. Diabetes. 2012;61(11):3018–25.
33. Wong FS, Karttunen J, Dumont C, Wen L, Visintin I, Pilip IM, et al. Identification of an MHC class I-restricted autoantigen in type 1 diabetes by screening an organ-specific cDNA library. Nature medicine. 1999;5(9):1026–31.
34. Leon S, Haguenauer-Tsapis R. Ubiquitin ligase adaptors: regulators of ubiquitylation and endocytosis of plasma membrane proteins. Experimental cell research. 2009;315(9):1574–83.
35. Zhang Z, Du J, Wang S, Shao L, Jin K, Li F, et al. OTUB2 Promotes Cancer Metastasis via Hippo-Independent Activation of YAP and TAZ. Molecular cell. 2019;73(1):7–21 e7.
36. Li J, Cheng D, Zhu M, Yu H, Pan Z, Liu L, et al. OTUB2 stabilizes U2AF2 to promote the Warburg effect and tumorigenesis via the AKT/mTOR signaling pathway in non-small cell lung cancer. Theranostics. 2019;9(1):179–95.
37. Chang W, Luo Q, Wu X, Nan Y, Zhao P, Zhang L, et al. OTUB2 exerts tumor-suppressive roles via STAT1-mediated CALML3 activation and increased phosphatidylserine synthesis. Cell reports. 2022;41(4):111561.
38. Beck A, Vinik Y, Shatz-Azoulay H, Isaac R, Streim S, Jona G, et al. Otubain 2 is a novel promoter of beta cell survival as revealed by siRNA high-throughput screens of human pancreatic islets. Diabetologia. 2013;56(6):1317–26.
39. Thomaidou S, Kracht MJL, van der Slik A, Laban S, de Koning EJ, Carlotti F, et al. β-Cell Stress Shapes CTL Immune Recognition of Preproinsulin Signal Peptide by Posttranscriptional Regulation of Endoplasmic Reticulum Aminopeptidase 1. Diabetes. 2020;69(4):670–80.
40. Loaiza Naranjo JD, Bergot AS, Buckle I, Hamilton-Williams EE. A Question of Tolerance-Antigen-Specific Immunotherapy for Type 1 Diabetes. Current diabetes reports. 2020;20(12):70.
41. Zheng L, Li J, Lenardo M. Restimulation-induced cell death: new medical and research perspectives. Immunological reviews. 2017;277(1):44–60.

42. Cho HI, Barrios K, Lee YR, Linowski AK, Celis E. BiVax: a peptide/poly-IC subunit vaccine that mimics an acute infection elicits vast and effective anti-tumor CD8 T-cell responses. Cancer immunology, immunotherapy: CII. 2013;62(4):787–99.
43. Zhang M, Wang S, Guo B, Meng G, Shu C, Mai W, et al. An altered CD8(+) T cell epitope of insulin prevents type 1 diabetes in humanized NOD mice. Cellular & molecular immunology. 2019;16(6):590–601.
44. Bassani-Sternberg M, Barnea E, Beer I, Avivi I, Katz T, Admon A. Soluble plasma HLA peptidome as a potential source for cancer biomarkers. Proceedings of the National Academy of Sciences of the United States of America. 2010;107(44):18769–76.
45. Laumont CM, Daouda T, Laverdure JP, Bonneil E, Caron-Lizotte O, Hardy MP, et al. Global proteogenomic analysis of human MHC class I-associated peptides derived from non-canonical reading frames. Nature communications. 2016;7:10238.
46. Son YI, Egawa S, Tatsumi T, Redlinger RE, Jr., Kalinski P, Kanto T. A novel bulk-culture method for generating mature dendritic cells from mouse bone marrow cells. Journal of immunological methods. 2002;262(1–2):145–57.
47. Trembleau S, Penna G, Gregori S, Chapman HD, Serreze DV, Magram J, et al. Pancreas-infiltrating Th1 cells and diabetes develop in IL-12-deficient nonobese diabetic mice. Journal of immunology. 1999;163(5):2960–8.
48. Jedema I, van der Werff NM, Barge RM, Willemze R, Falkenburg JH. New CFSE-based assay to determine susceptibility to lysis by cytotoxic T cells of leukemic precursor cells within a heterogeneous target cell population. Blood. 2004;103(7):2677–82.
49. Schatton T, Murphy GF, Frank NY, Yamaura K, Waaga-Gasser AM, Gasser M, et al. Identification of cells initiating human melanomas. Nature. 2008;451(7176):345–9.
50. Posch C, Moslehi H, Feeney L, Green GA, Ebaee A, Feichtenschlager V, et al. Combined targeting of MEK and PI3K/mTOR effector pathways is necessary to effectively inhibit NRAS mutant melanoma in vitro and in vivo. Proceedings of the National Academy of Sciences of the United States of America. 2013;110(10):4015–20.

Figures

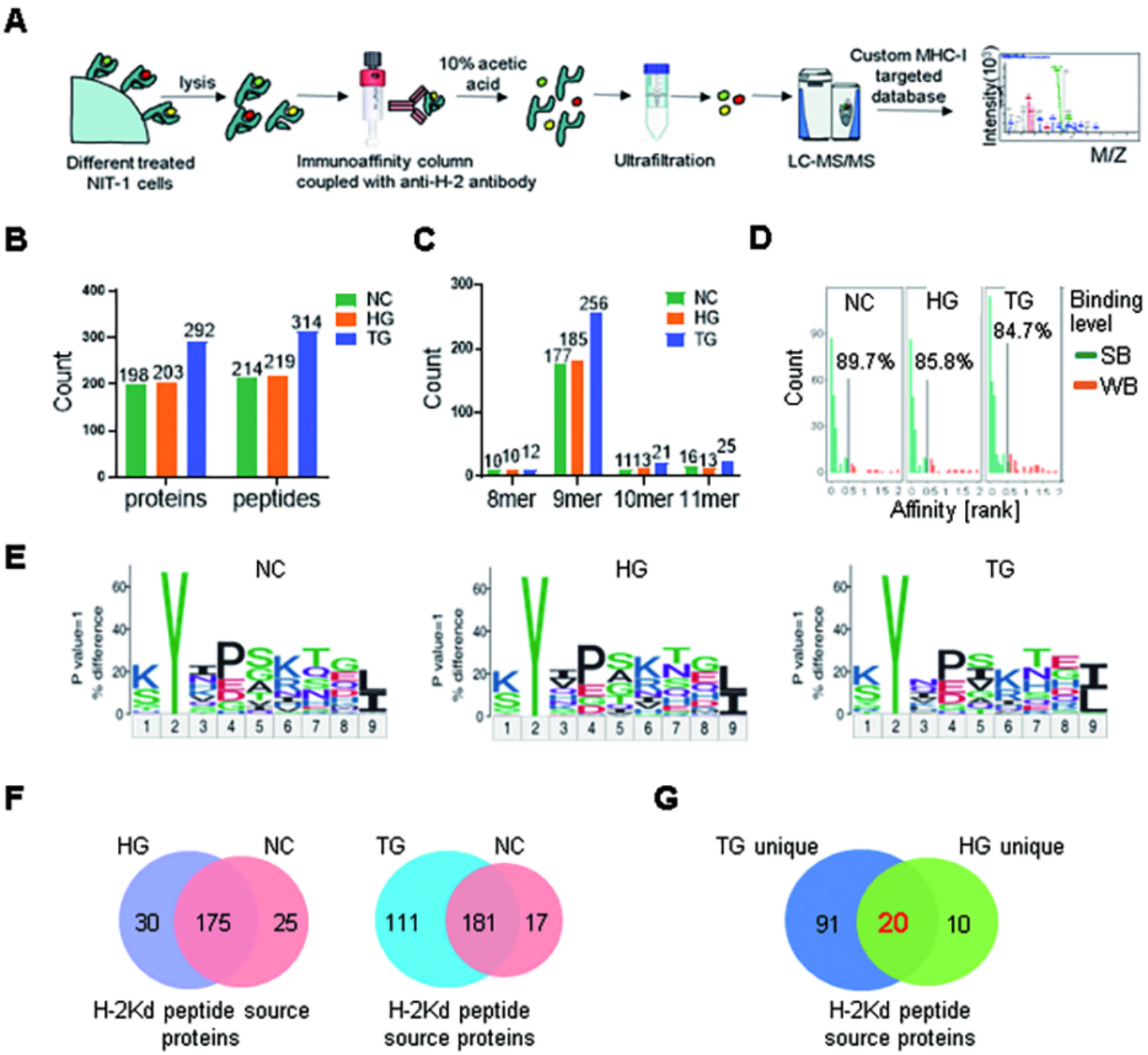

Figure 1

HG and TG treatment reshapes the NIT-1 cell-derived MIP. **A**The workflow for NIT-1 cell-derived MIP identification. **B** The total numbers of H2-Kd-restrictedpeptides and their potential source proteins in the MIP derived from NIT-1-NC, NIT-1-HG and NIT-1-TG cells. **C** The length distributions of MIP derived from NIT-1-NC, NIT-1-HG and NIT-1-TG cells (8-11 amino acids). **D** The predicted affinities of peptides by netMHC (version 4.0), SB: strong binder (rank<0.5%); WB: weak binder (rank:0.5%-2%). **E** The binding motifs of 9-mer peptides identified in the MIP. The x-axis represents the residue position within the 9-mer peptide sequence. The y-axis represents the information content, with the size of each amino acid symbol proportional to its frequency. **F** Overlap of the H-2Kd-restricted MIP between NIT-1-NC and NIT-1-

HG cells and between NIT-1-NC andNIT-1-TG cells at thesource proteinlevel. **G** Overlap of the source proteins for H-2Kd-restricted peptides exclusively present in the MIPof NIT-1-HG and NIT-1-TG cells.

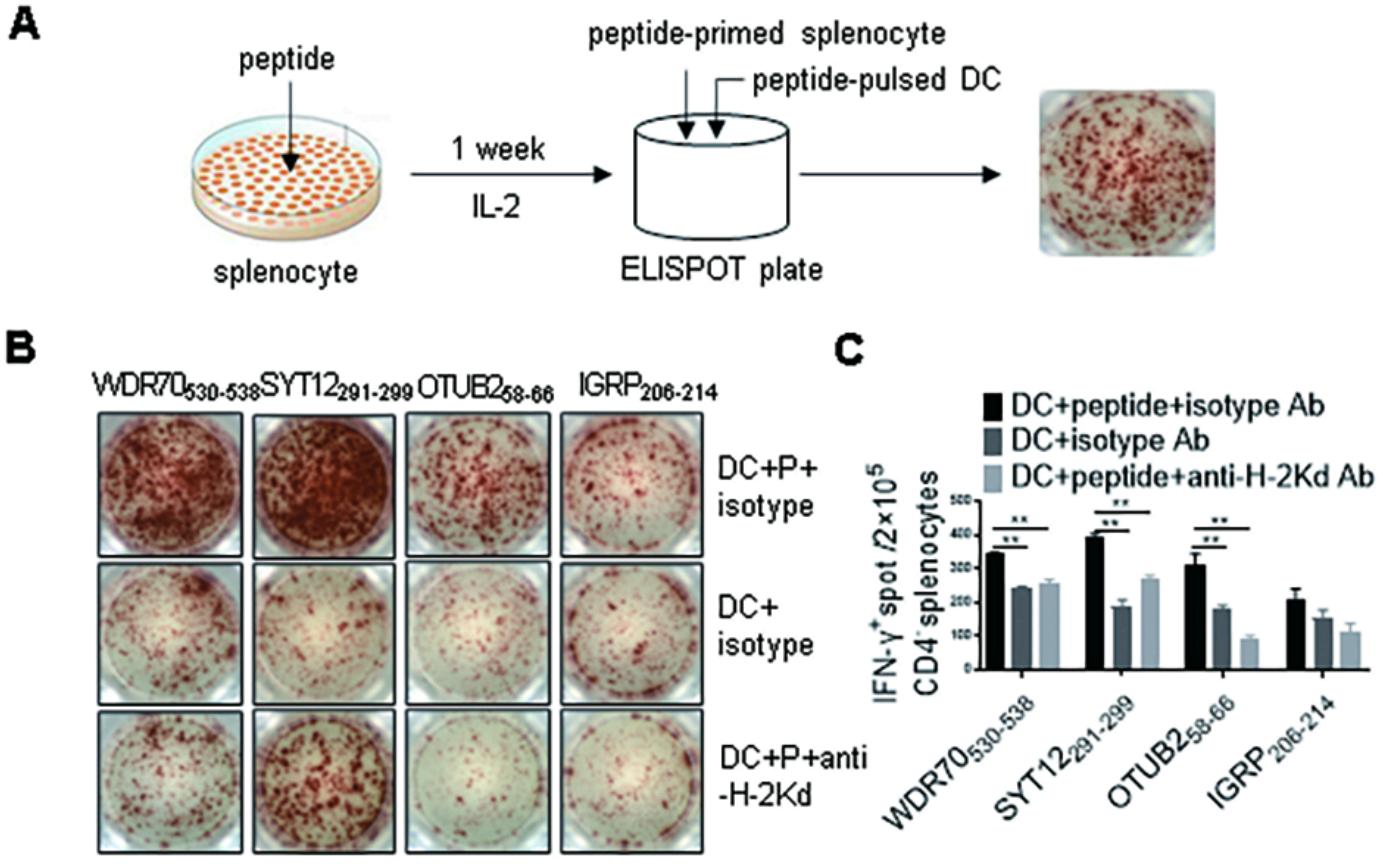

D

		5-13 weeks NOD mouse (n=8)								% positive
		M1(5w)	M2(5w)	M3(6w)	M4(6w)	M5(8w)	M6(9w)	M7(12w)	M8(13w)	
	$WDR70_{530-538}$	119.5	183.5	ND	156	343	79.5	149	162	
$WDR70_{530-538}$	Basal + 3SD	165.4	159	ND	190.6	253.5	55.9	56.1	230.8	57.1 (4/7)
	Basal	123	142	ND	188.5	245	49.5	45.5	173.5	
	$SYT12_{291-299}$	117	138	ND	128	390.5	164.5	214.5	216	
$SYT12_{291-299}$	Basal + 3SD	161.2	144.2	ND	149.6	250.64	70.9	174.2	207.2	57.1 (4/7)
	Basal	106	140	ND	147.5	187	64.5	119	186	
	$OTUB2_{58-66}$	160.5	185	219.5	140	312.5	265	152	267.5	
$OTUB2_{58-66}$	Basal + 3SD	129.4	139.5	199.2	162	215.2	54.9	102.1	234.7	87.5 (7/8)
	Basal	87	131	195	145	177	48.5	57.5	205	
	$IGRP_{206-214}$	ND	ND	117	ND	208.5	94.5	ND	425.5	
$IGRP_{206-214}$	Basal + 3SD	ND	ND	292.5	ND	225.8	107.2	ND	316.6	25 (1/4)
	Basal	ND	ND	205.5	ND	151.5	86	ND	280.5	

Figure 2

$OTUB2_{58-66}$ is an immunodominant self-peptide in NOD mice. **A** The workflow for the recall IFN-γ ELISPOT assay. **B** Representative ELISPOT images showing IFN-γ production by the indicated peptide-primed NOD mouse $CD4^-$ splenocytes restimulated with DCs plus an isotype control antibody

(DC+isotype), indicated peptide-pulsed DCs plus the isotype control antibody (DC+P+isotype) or indicated peptide-pulsed DCs plus an anti-H-2Kd antibody (DC+P+anti-H-2Kd). **C** Summary data for the assay in (B) showing the mean IFN-γ spot number per 2×10^5 $CD4^-$ splenocytes ± SD in duplicate cultures of one representative experiment. *p < 0.05, **p < 0.01 by Student's t test. **D** The reactivity of $CD4^-$ splenocytes from NOD mice harvested at different weeks of age against the indicated peptides, as determined by the recall IFN-γ ELISPOT assay. Readouts are expressed as the mean spot numbers/2×10^5 $CD4^-$ splenocytes in duplicate cultures. The average readout from $CD4^-$ splenocytes restimulated with DCs alone was set as the basal response. A positive response against the indicated peptide was defined as readouts above basal + 3SD (underlined); ND indicates no data.

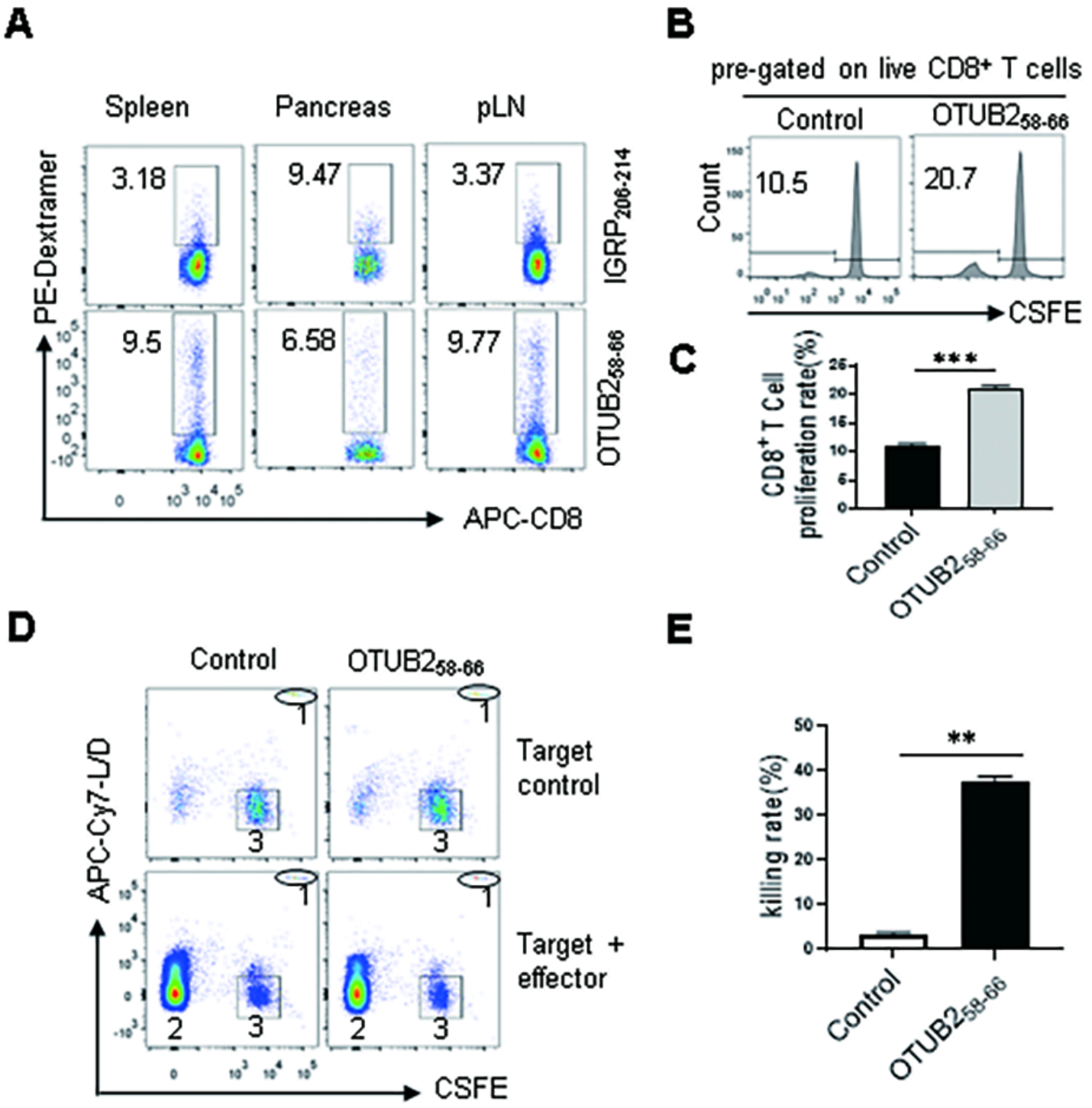

Figure 3

Characterization of $OTUB2_{58-66}$-specific $CD8^+$ T cells in NOD mice. **A** Representative FACS plots of $CD8^+Dextramer^+$ T cells in the spleen, pancreas and pLN of NOD mice. **B** Representative FACS histograms showing CFSE dilution in NOD mouse splenic $CD8^+$ T cells stimulated with or without $OTUB2_{58-66}$. **C** Summary data for the assay in (B) are presented as the mean proliferation rate ±SD in triplicate for one representative result of three independent experiments. **D** Representative FACS plots of

peptide-loaded or unloaded NOD mouse splenocytes labeled with CFSE and incubated for 4 hours in the presence (target + effector) or absence (target control) of NOD mouse $CD8^+$ T cells (E/T ratio, 100:1). Population 1 contained fluorescent microspheres that could be discriminated on the basis of their scattering pattern and fluorescence. Population 2 contained CFSE-negative cells (effector T cells). Population 3 contained CFSE-positive cells (target cells). **E** Summary data for the assay in (D) are presented as the mean killing rate ± SD in triplicate for one representative result of three independent experiments. **P<0.01, ***p < 0.001 by Student's t test.

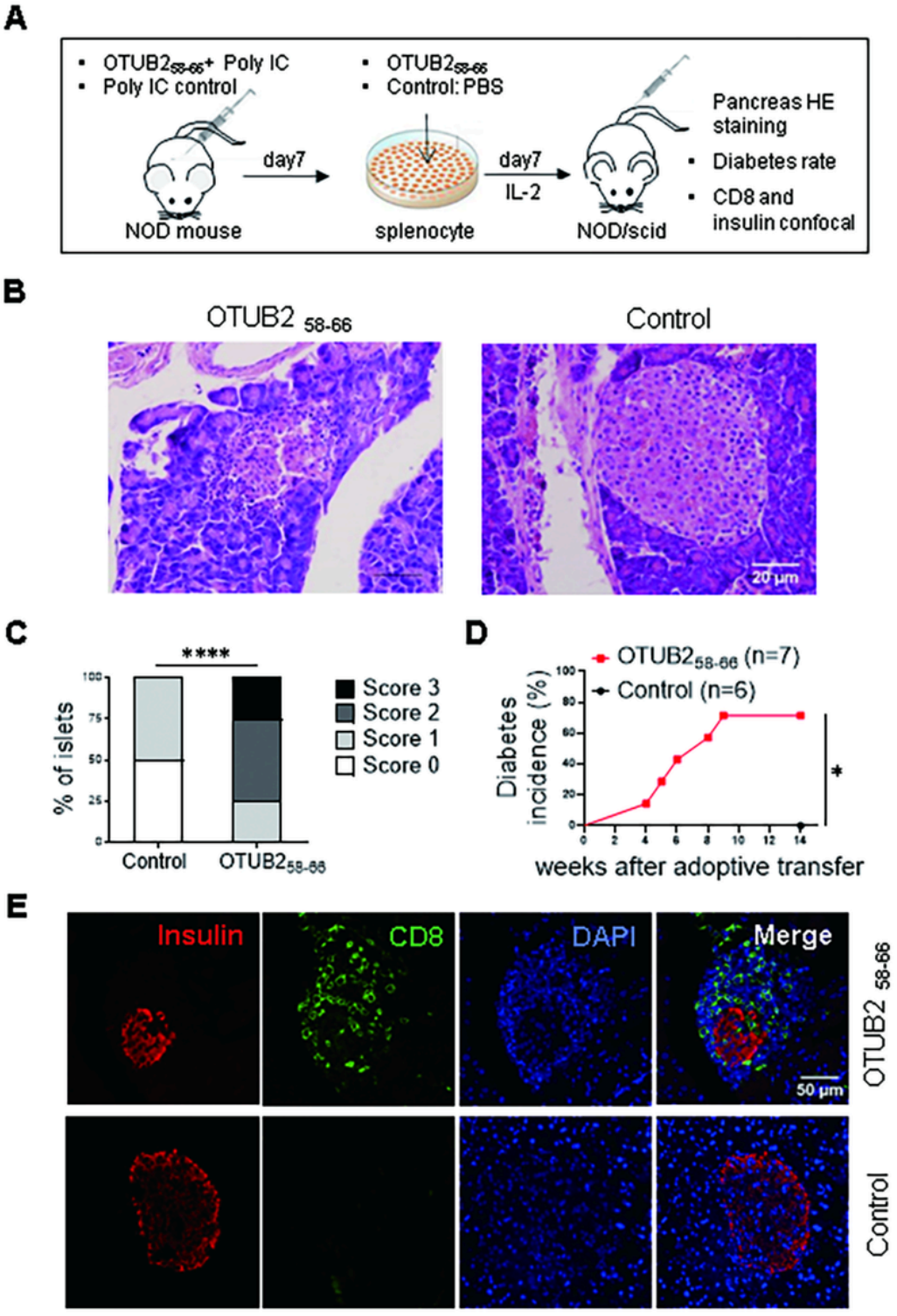

Figure 4

$OTUB2_{58\text{-}66}$ peptide-specific $CD8^+$ T cells are diabetogenic in NOD/scid mice. **A** The workflow for the adoptive transfer experiment. **B** Representative images of HE staining of the pancreas of NOD/scid mice receiving $OTUB2_{58\text{-}66}$-activated or control splenocytes (magnification, 200×). **C** Insulitis scores of NOD/scid recipient mice receiving $OTUB2_{58\text{-}66}$-activated or control splenocytes. **D** T1D incidence curve of NOD/scid mice adoptively transferred with $OTUB2_{58\text{-}66}$-activated or control splenocytes. Significance was determined by the log-rank (Mantel–Cox) test, *P<0.05. **E** Representative laser confocal fluorescence microscopy images of NOD/scid mouse pancreatic sections stained for insulin (red) and CD8 (green). Cells were counterstained with the nuclear dye DAPI (blue).

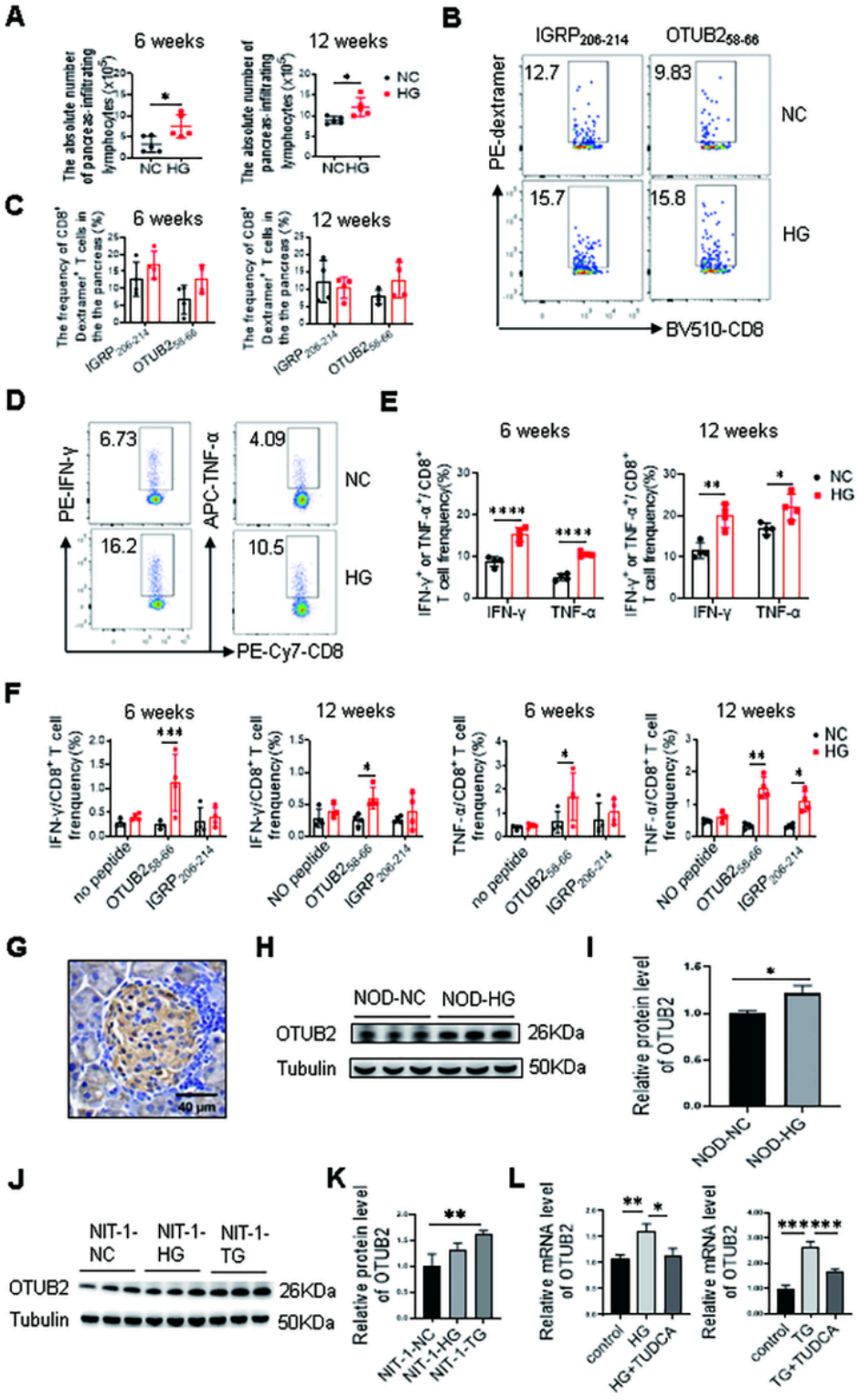

Figure 5

Sustained high glucose intake increases the peptide-specific $CD8^+$ T-cell response against $OTUB2_{58-66}$ in NOD mice. **A** Summary data showing the absolute cell number of pancreas-infiltrating lymphocytes in 6- and 12-week-old NOD mice fed high-glucose water (HG) or normal water (NC) (n=5 per group). **B** Representative FACS plots of $CD8^+$ $Dextramer^+$ T cells in the pancreas of 6-week-old NOD mice fed high-glucose water (HG) or normal water (NC). **C** Summary data for the assay in (B) are representative of

two independent experiments and presented as the mean ± SD (n=4 per group). **D** Representative FACS plots showing the production of IFN-γ and TNF-α by NOD mouse-derived splenic $CD8^+$ T cells stimulated with PMA. **E** Summary data for the assay in (D) are representative of two independent experiments and presented as the mean ± SD (n=4 per group). **F** Summary data showing the frequencies of IFN-γ- and TNF-α-producing cells in 6- and 12-week-old NOD mouse splenocytes stimulated or not with the indicated peptide. Data are expressed as the mean ± SD, n=4. **G** Representative image of immunohistochemical analysis of OTUB2 expression in pancreatic sections from NOD mice. **H-I** Western blot analysis of OTUB2 expression in the pancreas of NOD mice given normal water (NC-NOD) or high-glucose water (HG-NOD). **J-K** Western blot analysis of the protein level of OTUB2 in untreated NIT-1 cells (NIT-1-NC) and NIT-1 cells treated with HG (NIT-1-TG) or TG (NIT-1-TG). **L** Quantitative PCR analysis of OTUB2 relative mRNA expression in untreated NIT-1 cells (control), NIT-1 cells treated with HG or TG, and NIT-1 cells treated in the presence of TUDCA. Data are representative of three independent experiments and expressed as the mean ± SD (n=3). *P<0.05, **P<0.01, ***p < 0.001, ****p < 0.0001, determined by Student's t test.

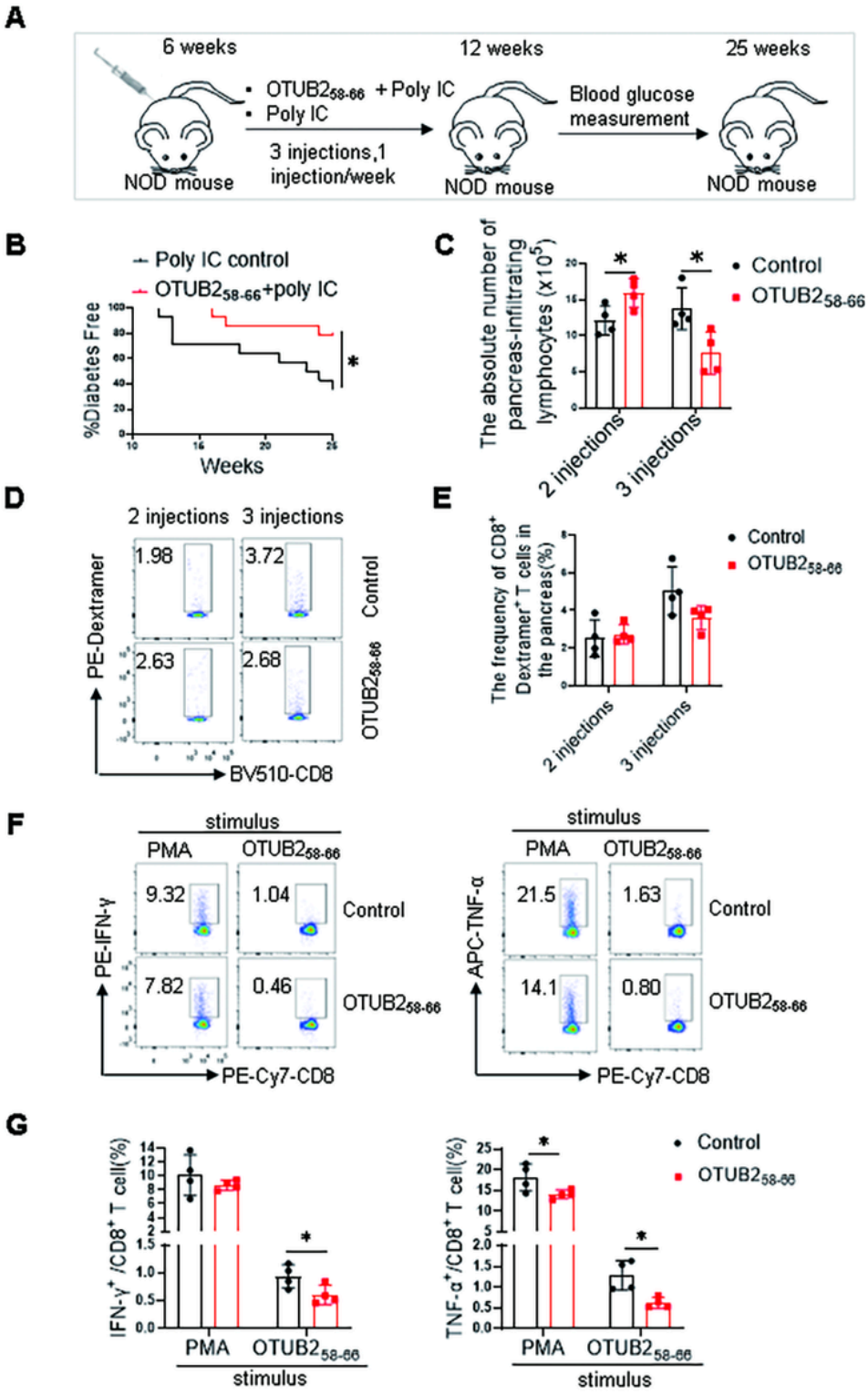

Figure 6

Repeated vaccination with the OTUB2$_{58-66}$ peptide prevents T1D onset in NOD mice. **A** The workflow for the peptide vaccination experiment. **B** Incidence of diabetes in female NOD mice injected with the OTUB2$_{58-66}$ peptide plus poly IC (red line, n = 14) or with poly IC alone (black line, n = 14). *p <0.05 compared by the log-rank (Mantel–Cox) test. **C** Summary data showing the absolute cell number of pancreas-infiltrating lymphocytes in NOD mice after 2 or 3 injections of the OTUB2$_{58-66}$ peptide mixed

with poly IC ($OTUB2_{58-66}$) or poly IC alone (Control). Data are representative of two independent experiments and presented as the mean ±SD (n=4 per group). **D** Representative FACS plots for $CD8^+Dextramer^+$ T cells in the pancreas of NOD mice after 2 or 3 injections of the $OTUB2_{58-66}$ peptide plus poly IC ($OTUB2_{58-66}$) or poly IC alone (Control). **E** Summary data for the assay in (D) showing the frequency of $CD8^+$ $Dextramer^+$ T cells in the pancreas of NOD mice after 2 or 3 injections. Data are representative of two independent experiments and presented as the mean ± SD (n=4 per group). **F** Representative FACS plots depicting PMA- and $OTUB2_{58-66}$-stimulated IFN-γ- and TNF-α-production by splenic $CD8^+$ T cells from NOD mice after 2 or 3 injections of the $OTUB2_{58-66}$ peptide plus poly IC ($OTUB2_{58-66}$) or poly IC alone (Control). **G** Statistics summary graph for the FACS analysis shown in (F). Data are representative of two independent experiments and presented as the mean ±SD (n=4 per group). *p <0.05, **p <0.01, ***p <0.001, determined by Student's t test.

Supplementary Files

This is a list of supplementary files associated with this preprint. Click to download.

- Supplementaltable1TotalpeptidesintheNIT1MIP.xlsx
- Supplementaltable2UniquepeptidesintheERSNIT1MIP.xlsx
- Supplementaryfigurelegends.docx
- FigS1.pptx
- figS2.tif
- figS3.tif
- FigS4.tif
- FigS5.tif
- FigS6.tif
- WBOriginalmap.pptx